

FULL PAPER

Kernel Estimates as General Concept for the Measuring of Pedestrian Density

Jana Vacková ^a and Marek Bukáček^a

^aFaculty of Nuclear Sciences and Physical Engineering, Czech Technical University in Prague, Prague, Czech Republic

ARTICLE HISTORY

Compiled May 23, 2022

ABSTRACT

The standard density definition produces scattered values. Hence approaches improving features of the density estimates has been invented for many use cases. Presented general framework evaluating density using various kernels brings desired properties of density estimates and incorporates the most of ordinarily used methods. Extensive parametric study is performed on experimental data to illustrate effects of kernel selection (e.g. Gauss, cone) and its parametrization (blur). Quantitative evaluation of introduced quality criteria illustrates that kernel densities satisfy user requirements, e.g. conic kernel with radius in $[0.7, 1.2]$ m. These parametric values are also interpretable from proxemic theory indicating correctness of the whole concept. Besides, the kernel approach is directly compared to Voronoi approximation and customized distance to the nearest pedestrian - the comparison indicates a relevant correspondence. Furthermore, the kernel approach is supposed to be valid from mathematical perspective, since introduced Borsalino kernel has promising mathematical properties enabling future analytical research.

KEYWORDS

Pedestrian dynamics; Density; Kernel functions; Minimum distance density; Voronoi diagram

1. Introduction

Flow, velocity and density are considered to be fundamental quantities in the both traffic flow, e.g. Treiber and Kesting (2013), and pedestrian dynamics, e.g. Daamen and Hoogendoorn (2007); Schadschneider et al. (2018). Although the first models discovering their essential relationship in a plain macroscopic way date back to 1960s, e.g. Underwood (1960), the optimal estimate of pedestrian density is still the contemporary topic in question.

The standard approach using physical definitions of flow and density as counting the number of pedestrians N passing through a cross-section within the interval ΔT or standing in the area A enriched by the hydrodynamic approximation

$$J = \frac{N}{\Delta T} \quad [\text{ped} \cdot \text{s}^{-1}], \quad \rho = \frac{N}{|A|} \quad [\text{ped} \cdot \text{m}^{-2}], \quad J = \rho \cdot v \quad (1)$$

was widely studied throughout the decades.

Although the fundamental definitions describe the current phase of the system, the numbers itself do not carry any specific information about the dynamics inside the system. It is possible to observe two configurations under very different internal conditions, however they both achieve the same value of (global) flow or (global) density, see Kerner (2004). Besides, sophisticated data analysis requires smoother data in time and space, simple counting cars or pedestrians brings scattered values with discrete jumps though.

Therefore researchers started to use approaches based on statistical methods (including kernel estimates) and even the methods where the expression of density is based on the time to collision or the minimum distance to another car or pedestrian. More general methods interpreting the pedestrian comfort or crowdedness as independent variables related to the density have become popular due to their greater relevance for several use cases. Development of the density estimates is discussed as follows.

Firstly, the smooth number of pedestrian in space and time was used in Helbing et al. (2006) and extended by the smooth contribution of one pedestrian in Helbing, Johansson, and Al-Abideen (2007), which was applied in Johansson et al. (2008); Johansson (2009). This definition is also an initial step to the individual density concept with dynamic detector in Bukáček and Vacková (2019).

Similar effect has the weighting of pedestrians mentioned in Schadschneider, Chowdhury, and Nishinari (2010); Schadschneider et al. (2018), including the density estimate defined as the body projection into the observed area in Predtetschenski and Milinski (1971) or by an inverse headway.

Very important paper Steffen and Seyfried (2010) about measuring fundamental quantities introduced the concept used in this paper. The properties of the standard definition (1) was discussed by authors in detail and the kernel approach was introduced. Authors considered several parametrized kernel types (Gaussian, conic, cylindrical) together with the approach of Voronoi diagram to estimate the density distribution in the observed area. Voronoi method was studied further then and stabilized by averaging over time in Liddle et al. (2011).

The comparison of different methods focusing on fundamental diagram was brought in Duives, Daamen, and Hoogendoorn (2015) covering weighted distance, estimates based on minimum distance to pedestrians or methods incorporating time spend in the detector. Another comparison of different methods (which are similar as the methods marked above) can be found also in Hillebrand, Hoogeveen, and Geraerts (2020) with the aim of the measuring of pedestrians safety.

Authors across all the mentioned papers agree that the disadvantage of using kernel approach is the calibration needed to scale parameter – in comparison to the popular non-parametric Voronoi approach.

Silverman (1986) solved this issue statistically using variance and interquartile range of the observations. However this kind of solution is not efficient due to the fact that the kernel parameter should be recomputed every single time step. Moreover, it is questionable whether the variance of pedestrian locations should control the kernel size in pedestrian density. Despite this, multiple researchers studied this approach – Krisp et al. (2009); Plaue et al. (2012); Plaue, Bärwolff, and Schwandt (2014); Mollier et al. (2019); Fan, Herty, and Seibold (2013); Fan (2013).

As noticed in most papers or conference presentations, it is not possible to choose a specific approach as the only correct one. Furthermore the parametrization may differ with an application. Nevertheless the chosen method significantly affects the

evaluation of quantities, from this reason it may have an impact on results, e.g. an examined phenomenon, like researchers already discussed – Schadschneider and Seyfried (2011); Hillebrand, Hoogeveen, and Geraerts (2020); Tordeux et al. (2015); Steffen and Seyfried (2010); Duives, Daamen, and Hoogendoorn (2015).

In our opinion, it is crucial to keep comparing methods in use and to identify common aspects as well as their differences. From our point of view, the density distribution based on kernel approach may be interpreted as a general concept, and therefore many other methods could be introduced only as its special cases. Moreover, the kernel approach (with an appropriate scaling) could be used as a good representative for multiple approaches mentioned above.

In this paper, we will firstly introduce several criteria for the quantification of the density estimate properties, thus the reader can precisely justify the application of studied methods. We will define the kernel concept then in a detail which non-kernel densities follow. And finally, we will present an experimental data-driven study of (dis)similarities between many methods mentioned earlier.

2. Methodology and Terminology

2.1. Measures

As we have already mentioned, the standard density definition (1) has several negative properties which make the density time series quite volatile.

To quantify this observation, we define mean absolute derivative understood as the *roughness* of the curve of the pedestrian count C and defined as follows

$$\langle \dot{C} \rangle := \frac{1}{\#T} \sum_{i=2}^{\#T} \frac{|C(t_i) - C(t_{i-1})|}{t_i - t_{i-1}} \quad [\text{ped/s}], \quad (2)$$

where $\#T$ denotes the total number of times (frames) that we have available from the experiment. Let us mention that $(t_i - t_{i-1})^{-1}$ as the frame rate is equal to 48 s^{-1} in our experiment.

On the other hand, any smoothing should not excessively decrease the range of the curve. This property is described by the maximum of the pedestrian count

$$\max_{t \in \mathbb{R}^+} C(t) \quad [\text{ped}], \quad (3)$$

which can be understood as the level of the *featureless*.

To simply describe any differences between two pedestrian counts, we use mean difference

$$\frac{1}{\#T} \sum_{i=1}^{\#T} (C_1(t_i) - C_2(t_i)) \quad [\text{ped}]. \quad (4)$$

2.2. The Conservation of the Mean Occupancy

Regardless of the drawbacks mentioned, the standard definition (1) produces solid macroscopic values. Thus any other (more or less exotic) approach should be close to the standard approach for sufficiently macroscopic and long term estimates. For instance, the mean occupancy of a detector (that is significantly larger in the comparison to pedestrian size) should be similar for all considered methods. As the mean occupancy is given by the mean time spent in the detector multiplied by the mean flow, i.e.

$$\langle N \rangle = \langle J \rangle \cdot \langle T \rangle = \langle J \rangle \cdot \frac{\ell}{\langle v \rangle}, \quad (5)$$

where $\langle \cdot \rangle$ denotes the mean value of a quantity and ℓ is the length of the detector; and the mean flow is given by the total number of passing pedestrians divided by the total time, i.e.

$$\langle J \rangle = \frac{N_{\text{tot}}}{t_{\text{max}} - t_0}, \quad (6)$$

the requirement to keep the mean occupancy in the detector is equivalent to the conservation of the mean flow, i.e. the total number of pedestrians. This requirement is evidently fulfilled due to the fact that we use the same input data. Let us note that is also satisfied following equality

$$\langle N \rangle = \frac{1}{t_{\text{max}} - t_0} \int_{t_0}^{t_{\text{max}}} N(t) dt = \frac{A}{t_{\text{max}} - t_0} \int_{t_0}^{t_{\text{max}}} \rho(t) dt = A \cdot \langle \rho \rangle. \quad (7)$$

From this reason we are vindicated to use the pedestrian count C instead of the density itself in our study. However note that

$$N_{\text{tot}} \neq \int_{t_0}^{t_{\text{max}}} N(t) dt. \quad (8)$$

To be specific

$$N_{\text{tot}} \cong \frac{\langle v \rangle}{\ell} \langle N \rangle (t_{\text{max}} - t_0). \quad (9)$$

2.3. Smoothing Techniques

The smoothing of density could be realized either by providing measurements which are less scatter; or by filtering of the final time series. To be more specific, these two options are:

- (1) **Spatial smoothing** which replace jump-like pedestrian contribution (as Dirac delta function) by a spatial representation of a person. This can be achieved by kernels, distance-weighted contributions or cell approach.
- (2) **Time smoothing** which balance rises and drops. This is achievable for example by (weighted) moving averages or any other filtration method conserving the mean value of observed time series.

As will be shown later, weighted moving averages (time smoothing) may be completely equivalent to kernel estimates (spatial smoothing) with respect to the assumption to pedestrian velocity or border conditions.

Both mentioned approaches can trivially replace density jumps caused by entering a new pedestrian into the detector, as visualized in Figure 1.

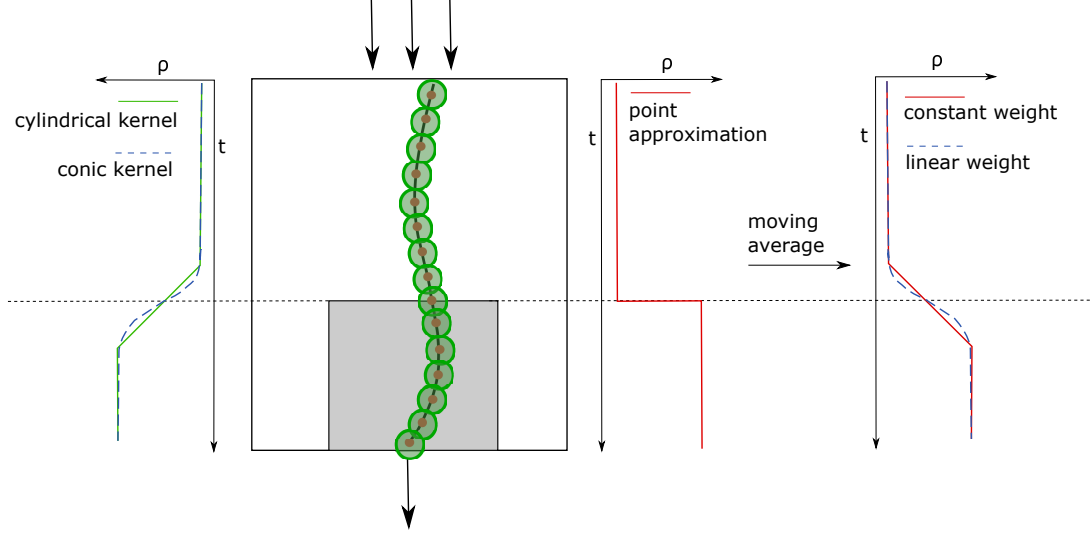


Figure 1. Equivalence of kernel approach (left) and point approximation processed by moving average (right).

3. Concept and Definition

Let us rewrite the definition of *density* in an area $A \subset \mathbb{R}^2$ using distribution inspired by kernel distribution theory, which is mentioned and study for instance in Wand and Jones (1994); Baszczyńska et al. (2016); Chacón and Duong (2018),

$$\rho = \frac{N}{|A|} = \frac{\int_A p(\mathbf{x}) d\mathbf{x}}{|A|} = \frac{\int_A \sum_{\alpha=1}^N p_{\alpha}(\mathbf{x}) d\mathbf{x}}{|A|} = \sum_{\alpha=1}^N \frac{\int_A p_{\alpha}(\mathbf{x}) d\mathbf{x}}{|A|}, \quad (10)$$

where N represents the number of pedestrians, $|A|$ the size of considered area A , $p_{\alpha}(\mathbf{x})$ the *individual density distribution* generated by each pedestrian $\alpha \in \{1, 2, \dots, N\}$ and

$$p(\mathbf{x}) = \sum_{\alpha=1}^N p_{\alpha}(\mathbf{x}) \quad (11)$$

defines the *density distribution* in the area A .

In a case that (sub)area A fills the whole examined area, the individual density distribution holds normalization condition

$$\int_A p_{\alpha}(\mathbf{x}) d\mathbf{x} = 1. \quad (12)$$

Therefore the relation $\int_A p(\mathbf{x}) d\mathbf{x} = N$ is fulfilled and the density ρ_A is called *global*.

To emphasize the generality of relation (10), we can write the definition of the density including kernel parameters

$$\rho_A = \frac{\int_A \sum_{\alpha=1}^N p_\alpha(\mathbf{x}, R) d\mathbf{x}}{|A|}. \quad (13)$$

Regardless the kernel type, R expresses the smoothing factor, thus we refer it as *blur*.

Blur R controls the size of an area affected by one pedestrian. Let us denote this area as the pedestrian *support* $A_\alpha \subset A$ and define as follows

$$A_\alpha = \{\mathbf{x} \in A \mid p_\alpha(\mathbf{x}) > 0\}, \quad (14)$$

i.e. A_α is the smallest possible subset of A fulfilling $\int_{A_\alpha} p_\alpha(\mathbf{x}) d\mathbf{x} = 1$.

When an area $B \subset A$ covers only a part of the possible area $A \subset \mathbb{R}^2$, i.e. $B \cap A \neq \emptyset$ and $B \cap A \neq A$, the pedestrian α may contribute to the density ρ_B only partially in case that $A_\alpha \cap B \neq A_\alpha$, i.e. $\int_B p_\alpha(\mathbf{x}) d\mathbf{x} < 1$.

If the kernels intersect the walls or obstacles, they are normalized to keep pedestrian volume in the eligible area, i.e. their support A_α is trimmed and the kernel is re-scaled to fulfil the normalization condition (12) – therefore the peak of the individual density distribution will be higher than in the case of non-intersection.

To be complete, the area A does not have to be static (a detector approach) like in Steffen and Seyfried (2010) – it can be variable in time. If the dynamic detector focuses on the surroundings of pedestrian α , we named the density *individual* and we have studied it for preliminary results in Bukáček and Vacková (2019); Vacková and Bukáček (2019). For clarity, let denote ω_α as the surroundings of pedestrian α . Then we note $\rho_{\omega_\alpha}(\mathbf{x})$ as the *individual density of pedestrian α* , in contrast to the *static detector density* $\rho_A(\mathbf{x})$ which will be the main topic of this paper.

3.1. Type of Kernels

If the surroundings is set to the whole considered area and Dirac delta function is used as the individual density distribution, the standard approach (1) is obtained. However there is more different choices of kernels as the individual density distribution. Denoting $\mathbf{x}_\alpha := \mathbf{x}_\alpha(t)$ as the (head) position of pedestrian α at fixed time $t \in \mathbb{R}_0^+$, let us mention a few of them which will be used in the further analysis.

3.1.1. Point Approximation

Already mentioned *Dirac delta function*

$$p_\alpha(\mathbf{x}) = \delta_{\mathbf{x}, \mathbf{x}_\alpha} \quad (15)$$

represents the point approximation of pedestrian distribution.

3.1.2. Stepwise function

The stepwise function can also be used, defined as follows

$$p_\alpha(\mathbf{x}, R) = \mathbb{1}_{A_\alpha(R)}(\mathbf{x}) \frac{1}{|A_\alpha(R)|}, \quad (16)$$

where symbol $\mathbb{1}_X$ represents the indicator function of set X and $A_\alpha(R)$ is the support of the pedestrian α . The shape of this area is chosen arbitrarily, we choose the *cylindrical kernel*, i.e.

$$A_\alpha(R) = \{\mathbf{x} \in \mathbb{R}^2 : \|\mathbf{x} - \mathbf{x}_\alpha\| \leq R\} \quad (17)$$

and

$$\mathbb{1}_{A_\alpha(R)}(\mathbf{x}) = \Theta(R - \|\mathbf{x} - \mathbf{x}_\alpha\|). \quad (18)$$

3.1.3. Conic Kernel

Conic kernel uses the same pedestrian support (17) and indicator function (18) as the cylindrical kernel, however with linear trend (not the constant as previously)

$$p_\alpha(\mathbf{x}, R) = \frac{3}{\pi R^3} \mathbb{1}_{A_\alpha(R)}(\mathbf{x}) (R - \|\mathbf{x} - \mathbf{x}_\alpha\|). \quad (19)$$

It has several desired features for representing pedestrians compared to the stepwise kernels, e.g. decreasing trend with increasing distance, limited support and the independence of one pedestrian to the others.

3.1.4. Borsalino Kernel

Borsalino kernel comes from Krbálek and Krbálkova (2018) where it is defined for one dimension. Generalization used in this paper for two dimensions can be defined as follows

$$p_\alpha(\mathbf{x}, R) = \frac{1}{Z} \frac{1}{R} \mathbb{1}_{A_\alpha(R)}(\mathbf{x}) \exp \left\{ \frac{R^2}{\|\mathbf{x} - \mathbf{x}_\alpha\|^2 - R^2} \right\} \quad (20)$$

with the same pedestrian support (17) and indicator function (18) as in the previous cases and normalization constant Z which is numerically calculated. This kernel has similar properties as the conic kernel. However they differ in theoretical features - Borsalino kernel is differentiable and this fact can be helpful in analytical calculations. On the contrary, the conic kernel does not have to be normalized using numerical computation. More about their differences with respect to the evaluating of densities will be found in further text.

3.1.5. Gaussian Kernel

We use Gaussian kernel in its symmetric version, i.e. with diagonal covariance matrix,

$$p_\alpha(\mathbf{x}, R) = \frac{1}{2\pi R^2} \exp \left\{ -\frac{\|\mathbf{x} - \mathbf{x}_\alpha\|^2}{2R^2} \right\}. \quad (21)$$

This is the only representative with a limitless area of influence (i.e. with unbounded pedestrian support) in this study. Blur parameter R represents the kernel bandwidth in our study, thus it is comparable through all used kernel shapes.

We work with kernels in their symmetric version here. It does not have to be this way in general, though. Furthermore the kernel size can be definitely enhanced by

varying in time in accordance with the conditions in pedestrian surroundings. We will not cover that in this study, it is the main point of the following research.

3.2. Non-Kernel Densities

Having defined the kernel concept, we need to present non-kernel methods for their comparison.

3.2.1. Voronoi Diagram

Voronoi diagram can be understood as a specific kind of kernel which is influenced by kernels around.

Each spatial point $\mathbf{x} \in \mathbb{R}^2$ is assigned to the nearest pedestrian α at position \mathbf{x}_α . The set of these points is called Voronoi cell in Steffen and Seyfried (2010) and it is denoted as A_α for pedestrian α . Thus the area A_α may be interpreted as the pedestrian support as it was in the context above. However A_α does not depend on any blur parameter R here.

It is possible to use a supplementary parameter as an upper boundary of the size of the Voronoi cell like it is discussed in Steffen and Seyfried (2010). Nevertheless we do not implement this kind of parameter in our study - it would have a different meaning (maximum blur) than a simple blur of pedestrian used in other kernels, thus it would not have been comparable. Beside that the maximum blur would influence only the low occupied room, i.e. only the beginning of density time series under conditions of our experiment. However it is necessary to think about usage the maximum blur in general situations.

We have to remark that the authors Steffen and Seyfried (2010) summed in the relation (10) Voronoi cells of pedestrians that lie inside the detector at least by a part of their Voronoi cells (the sum is greater than real contained mass), or Voronoi cells of pedestrians that lie inside the detector (the sum is lower than real contained mass). We use here the accurate sum of the part of Voronoi cells lying inside the detector - not less, not more. The situation is depicted in Figure 2.

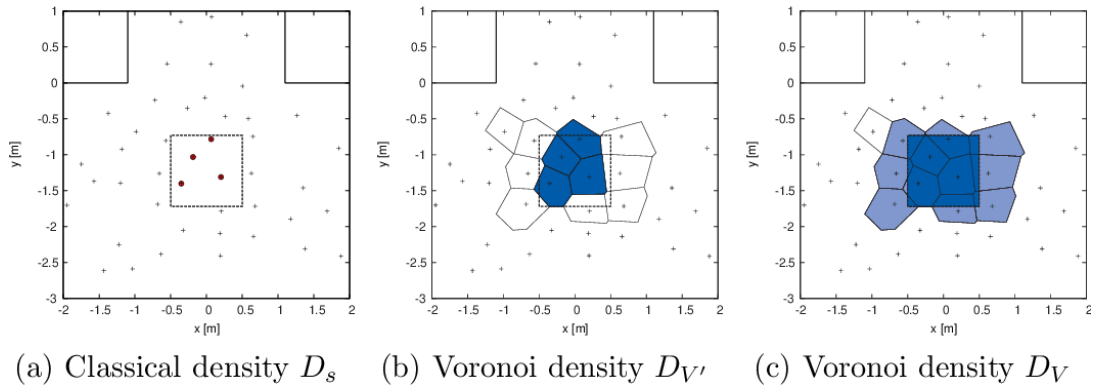


Figure 2. Using Voronoi diagram according to Steffen and Seyfried (2010). Figure is taken from Steffen and Seyfried (2010).

3.2.2. Minimum Distance Estimate

Let us imagine that we are in an one-dimensional space, where we can write the standard definition (1) of the density as $\rho = N/x$ with number of agents $N \in \mathbb{N}$ and the length of the interval $x \in \mathbb{R}$. It can be rewritten using mean headway between consecutive agents $\rho = 1/\langle x \rangle$. We can conclude that if we want to find maximum density, we need to find the minimum possible mean headway. Hence the highest density that can be measured is the density obtained by the estimate $\rho_{\text{worst}} \approx 1/\min\langle x \rangle$.

However we operate in two dimensions in pedestrian dynamics. We rewrite it then similarly as $\rho = 1/\langle |A| \rangle$ where $\langle |A| \rangle$ can be imagined as the size of mean area occupied or hold by one pedestrian, i.e. mean area A_α over possible pedestrians α . From this reason, we can approximate it as a circle with radius equal to mean distance to the neighbour, i.e. $\langle |A| \rangle = \pi \langle x \rangle^2$. This means that the highest density is again connected with the minimum distance to a neighbour.

We define the density distribution (at every time) as

$$p(\mathbf{x}) = \frac{c_{md}}{\text{dist}(\mathbf{x})}, \quad (22)$$

where $c_{md} \in \mathbb{R}^+$ represents a calibration constant. We will be examining two options for the function $\text{dist}(\mathbf{x})$.

According to Duives, Daamen, and Hoogendoorn (2015), we will use minimum distance measure with the specific field of vision

$$\text{dist}(\mathbf{x}) := D(\mathbf{x}) := \min_{\{\alpha \in \mathbb{N} : \angle(\mathbf{x}_\alpha, \mathbf{s}_x) \leq \frac{\pi}{3}\}} \|\mathbf{x} - \mathbf{x}_\alpha\|, \quad (23)$$

where \mathbf{s}_x represents the direction from the current point $\mathbf{x} \in \mathbb{R}^2$ to the middle point of the exit. In Duives, Daamen, and Hoogendoorn (2015), there is the minimum distance density evaluated only in the pedestrian locations \mathbf{x}_α .

Differently from Duives, Daamen, and Hoogendoorn (2015), we evaluate the density distribution at every point in space. Thus we have to set the field of vision at every point in space, find the pedestrian which is the closest pedestrian to this point (if there is any) and count the value of the distribution. The angle of the pedestrian field of vision is chosen according to Duives, Daamen, and Hoogendoorn (2015) as 120 degrees, i.e. $2/3\pi$ radians.

Due to the two dimensional space where we operate, we are highly motivated to check our two-dimensional improvement of the previous distance measure defined as

$$\text{dist}(\mathbf{x}) := D(\mathbf{x})^2. \quad (24)$$

We are convinced that this kind of measure may bring better results, because we are aware of the approximation discussed above.

However we have to note that there are points which are not defined due to the avoiding of the infinity values of the distance measure, or due to the absence of any pedestrian in the field of vision from the specific point.

The example of density distribution for different kernels can be seen in Figure 3 and Figure 4.

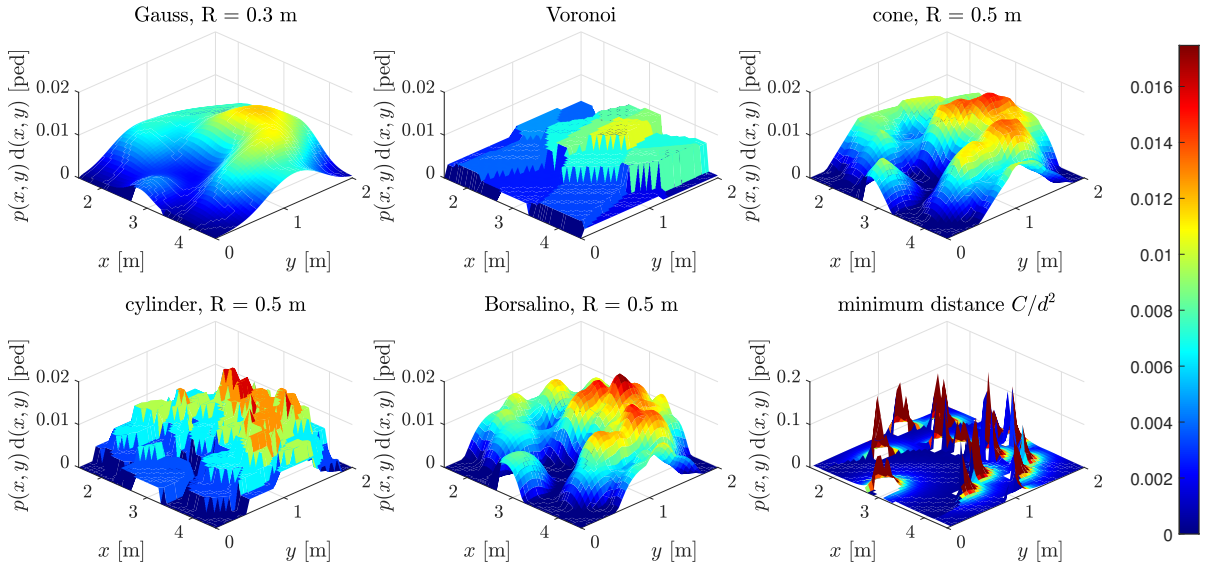


Figure 3. An example of density distributions (side view).

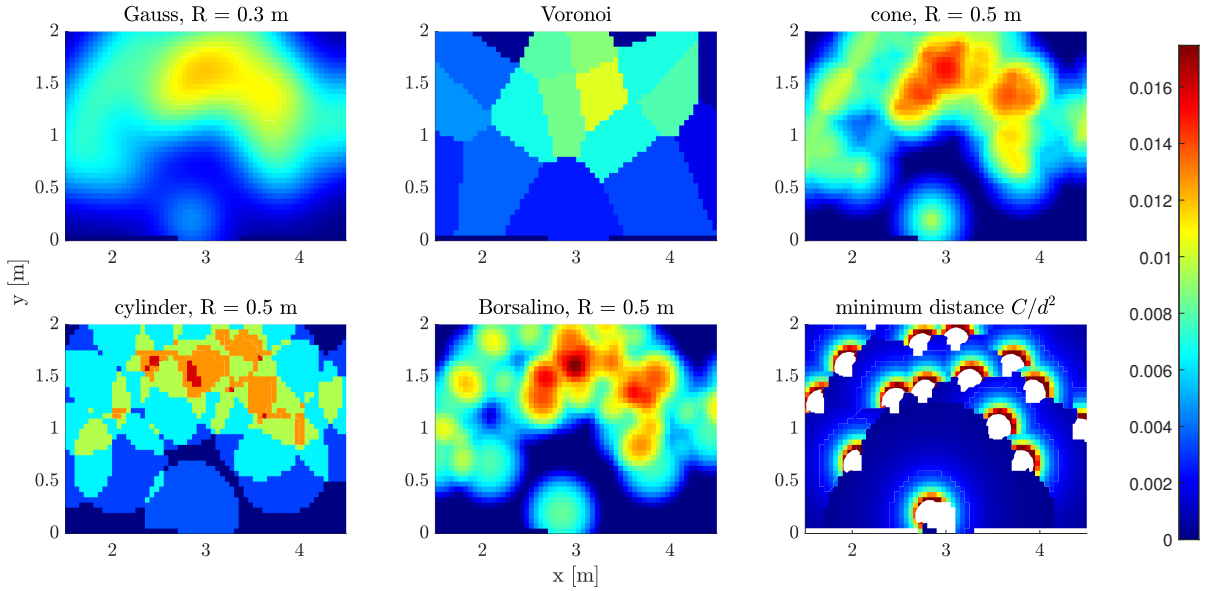


Figure 4. An example of density distributions (view from above).

4. Experimental Data-Driven Study

The following parametric study is based on the egress experiment organized in the study hall of FNSPE, CTU in Prague in 2014, for details see Bukáček, Hrabák, and Krbálek (2015, 2016, 2018). Pedestrians (undergraduate students wearing recognition caps) randomly entered the room by one of three entrances, walked to the opposite wall and left the room by one exit. By controlling input flow, different conditions from free flow to congestion in the exit area were achieved. In total, our sample is made up of 2000 paths through 10 experimental rounds captured using 48 frames per seconds.

In order to examine the kernel shape and size, the parametric study is based on a simple static detector visualized as the red rectangle area A in Figure 5

$$A := \{\mathbf{x} = (x_1, x_2) \in \mathbb{R}^2 : x_1 \in \langle 2, 4 \rangle \wedge x_2 \in \langle 0, 1 \rangle\}$$

and denote $\rho(t) := \rho_A(t)$ for simplicity in this section. Similarly we will use the variable called pedestrian count $C(t) := C_A(t)$ instead of the density where appropriate (see Section 2).

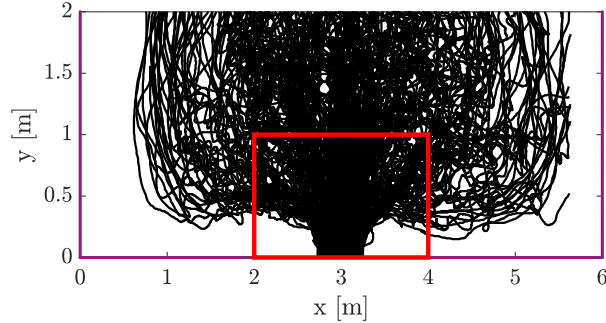


Figure 5. Trajectories in the round 6 of the experiment and chosen static detector (red rectangle).

To compare experimental rounds with different time length, the normalized time t_{norm} (in the meaning that the start is represented by $t_{norm} = 0$ and the end by $t_{norm} = 1$) will be used.

Conic, cylindrical, Gaussian and Borsalino kernels are evaluated for wide range of parameter $R \in \{0.1, 0.2, \dots, 3\}$ while Voronoi distribution, point approximation and minimum distance approach are evaluated only once (there is no parameter).

In our study, firstly, we will verify the possibility of conic kernel to copy all already mentioned density evaluation methods, then the quantitative comparison will be provided.

4.1. Convergence to Point Approximation

It is known from the theory of generalized functions

$$\lim_{R \rightarrow 0^+} p(\mathbf{x}, R) = \lim_{R \rightarrow 0^+} \sum_{\alpha=1}^N p_{\alpha}(\mathbf{x}, R) = \sum_{\alpha=1}^N \delta_{\mathbf{x}, \mathbf{x}_{\alpha}}, \quad (25)$$

i.e. the sum of individual density distributions converges to the sum of centralized Dirac delta functions into the pedestrian locations.

To illustrate this property, Figure 6 was prepared as the comparison of pedestrian count obtained by the point approximation and pedestrian count of an examined conic kernel, specifically the median value of pedestrian conic count for fixed value of pedestrian Dirac count. It is evident that the closer the axis of the first quadrant, the closer the Dirac count.

It is seen in Figure 6 that the conic count for blur $R = 0.1$ m is very similar to the Dirac count which is in accordance with the theoretical result. Moreover, the deviation between conic and Dirac count is greater for higher Dirac count and higher values of blur - the highest the blur and the Dirac count, the slope of the line is lower. This is

caused by the blending of the pedestrian outside the detector which is more significant for greater Dirac count.

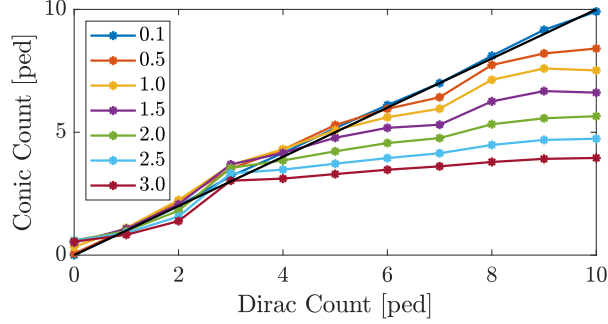


Figure 6. Similarity to point approximation.

4.2. Voronoi Alternatives

Having discussed the point approximation, it may be useful to realize if there is any parametric settings of kernels which is close to Voronoi pedestrian count. To measure this (dis)similarity, we choose total absolute deviation.

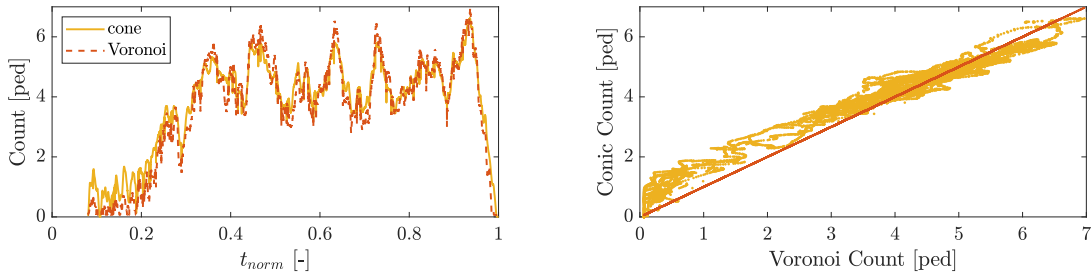


Figure 7. Conic alternative for $R = 1.6$ m of Voronoi diagram for experimental round number 6: time development (left), pedestrian count distribution (right).

Time development of pedestrian count (left) and pedestrian count distribution for different kernels versus Voronoi distribution (right) are denoted in Figure 7. We can conclude that Voronoi pedestrian count has its alternative in conic kernel, specifically for $R \in (1.5, 3)$ m - the value of R depends on the phase of the system (experimental round). However there is greater range for Voronoi than for cone and also slight differences for low densities in Figure 7 (left). This undervaluation of Voronoi pedestrian count is evident in Figure 7 (right) and caused by blending the pedestrian during free flow phases. The greater range could be caused by the property that Voronoi may resemble Dirac distribution under specific condition (dense crowd).

4.3. Recomputation of Gaussian Mass

We have already noticed e.g. from Figure 4 that Gaussian kernel gives us very similar distribution as conic kernel, however it seems to be more blurred which emerges from Gaussian limitless support. We would like to examine if any formula exists between Gaussian and conic kernel that it would erase this difference.

To reach our aim, it is necessary to get 'almost all' mass of Gaussian kernel into the base of the cone centralized at $\mathbf{0}$ denoted as $A_R = \{\mathbf{x} \in \mathbb{R}^2 : \|\mathbf{x}\| \leq R\}$. Let us denote Gaussian kernel at $\mathbf{0}$ with variance $\sigma^2 \in \mathbb{R}^+$

$$p(\mathbf{x}, \sigma) = \frac{1}{2\pi\sigma^2} e^{-\frac{\|\mathbf{x}\|^2}{2\sigma^2}}.$$

As we want to find relation between conic R and Gaussian σ , let assume that $R = k\sigma$, $k \in \mathbb{N}$. Thus we solved the following integral

$$\int_{A_R} p(\mathbf{x}, \sigma) d\mathbf{x} = \int_{A_{k\sigma}} p(\mathbf{x}, \sigma) d\mathbf{x} = \int_0^{\frac{k^2}{2}} e^{-t} dt.$$

The result is lower incomplete Gamma function which has numerically known values. These values are computed in Table 1 for $k \in \{1, 2, 3, 4\}$. For instance, Gaussian mass for $\sigma = \frac{R}{3}$ is inside the base of the cone with radius R by almost 99%. Thus their pedestrian counts are comparable which is depicted in Figure 8.

Table 1. Gaussian mass inside the base of cone for different values of k .

k [-]	1	2	3	4
mass [%]	39.35	86.47	98.89	99.97

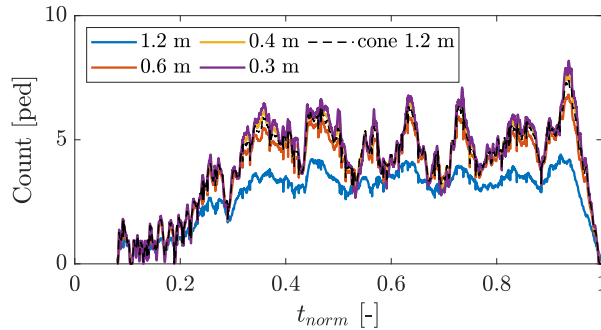


Figure 8. Gaussian and conic pedestrian counts in time for experimental round number 6 for different values of R .

4.4. Comparison of Conic and Borsalino Kernel

Finally we will compare two very similar kernels - conic kernel and Borsalino kernel. Considering the properties of these two functions (limited support, decreasing trend), we expect the similar behaviour. For this reason, we evaluated mean difference between pedestrian count of conic and Borsalino kernel according to (4) which can be seen in Figure 9 for different experimental rounds.

There is a dissimilarity between the experimental rounds with free flow phase (green) and other experimental rounds (transition - blue, stable cluster - magenta, congestion - red). Overall, the mean difference is very close to zero for all values of blur R - the greatest difference is quantified as less than -0.12 ped.

Thus we can conclude this section that conic kernel and Borsalino kernel generate almost identical densities. However, Borsalino kernel may work better for theoretical

studies due to its smoothness (infinitely differentiable).

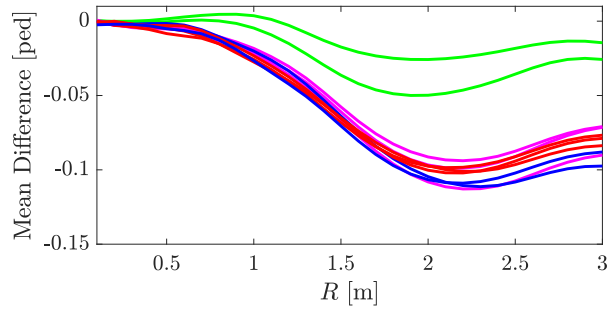


Figure 9. Mean difference between conic and Borsalino pedestrian count for all experimental rounds (free flow - green, transition - blue, stable cluster - magenta, congestion - red).

4.5. Comparison of Conic and Cylindrical Kernel

Similarly we examine also the mean difference of pedestrian count (4) for conic and cylindrical kernels. The result is seen in Figure 10 for all experimental rounds. Cone gives us greater pedestrian count than cylinder, especially for greater values of blur which is caused by the linear trend for cone and the constant trend for cylinder. However, the highest difference occurs less than 0.8 ped. To summarize, these kernels are very close for lower values of blur.

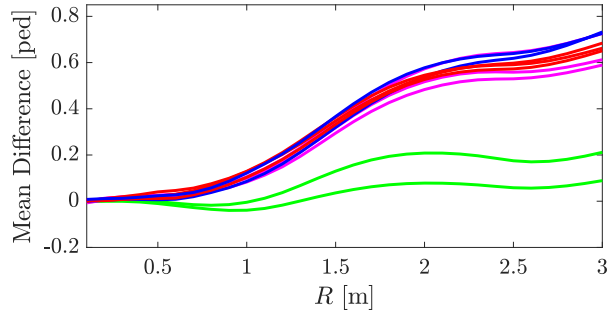


Figure 10. Mean difference between conic and cylindrical pedestrian count for all experimental rounds (free flow - green, transition - blue, stable cluster - magenta, congestion - red).

4.6. Comparison of Conic Kernel and Minimum Distance Estimate

Firstly, we have to calibrate the minimum distance distributions. As it is not the main goal of this paper, we will take it briefly without many details. The calibration process is separated according to the flow type and the calibration constant will might depend on the size of blur R . We have to ensure that the training and testing set contains every type of flow, thus we define the set in the following way: training set as round number 5, 4, 9 and 7 (free flow, transition, stable cluster, congestion), and testing set as round number 2, 6, 10 and 11 (in the same order as the training set).

The calibration metric is chosen as the absolute deviation of the conic pedestrian count and the pedestrian count of minimum distance distribution in the detector.

The calibration constant for minimum distance distribution $1/d^2$ with respect to R is depicted in Figure 11. To avoid this dependency on blur, we can approximate the function of calibration constant with respect to blur R by a constant function with the value belonging to $R = 0.9$ m which need to be made separately for free flow and other conditions. Finally, we found the calibration constant for minimum distance distribution $1/d$ as

$$c_{md}^{(1)} = \begin{cases} 0.0233 \text{ ped} & \dots & \text{free flow,} \\ 0.0400 \text{ ped} & \dots & \text{otherwise,} \end{cases} \quad (26)$$

and for minimum distance distribution $1/d^2$ as

$$c_{md}^{(2)} = \begin{cases} 0.1219 \text{ ped} & \dots & \text{free flow,} \\ 0.1628 \text{ ped} & \dots & \text{otherwise.} \end{cases} \quad (27)$$

The fit of calibrated distribution $1/d^2$ is shown on the testing set (using conic kernel with fixed R) in Figure 12. The correspondence between the curves is evident for every experimental round, i.e. different phases of the system.

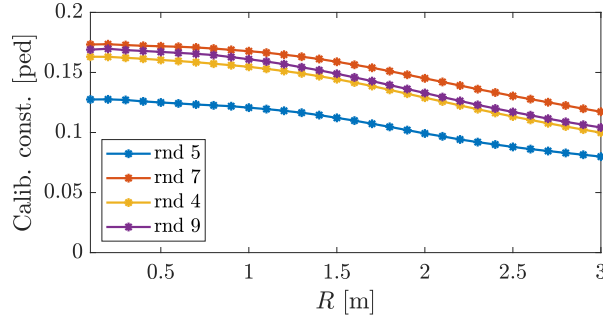


Figure 11. Calibration constant of minimum distance $1/d^2$ pedestrian count for different experimental rounds (training data).

Finally we have to note that this calibration process with respect to conic kernel is robust. If any kernel distribution is not available, the calibration process would be performed using Dirac distribution - however our process contains the Dirac distribution implicitly, see Section 4.1.

4.7. Final Quantitative Comparison

4.7.1. Time Development

We plotted the pedestrian count $C(t)$ for examined methods for $R \in \langle 0.1, 2 \rangle$ m (if it is possible) for round 6 of the experiment in Figure 13. We can see an essential difference between Gaussian kernel and the conic, cylindrical and Borsalino kernels which behave similarly. Gaussian kernel smooths the pedestrian count from $R = 1.5$ m significantly – it is caused by different scaling as explained in Section 4.3. Voronoi cannot be discussed in this way because it has no parameter to change. The similarity of the count generated by Voronoi diagram was discussed in Section 4.2 separately. Minimum distance estimate has no parameter either, however we have two calibrated options C/d and C/d^2 , for details see Section 4.6. It can be seen that the option C/d^2

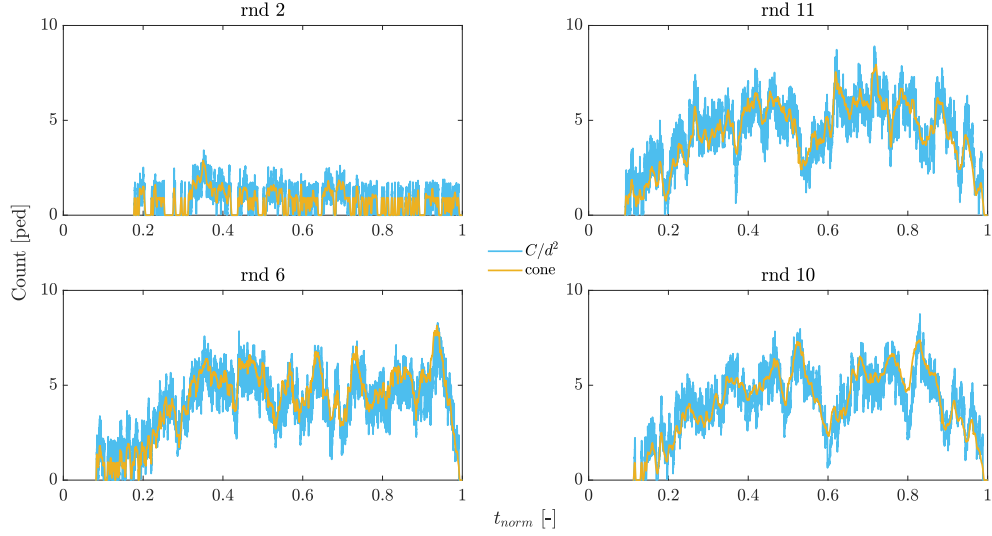


Figure 12. Calibrated minimum distance $1/d^2$ pedestrian count versus conic pedestrian count ($R = 0.9$ m) for different experimental rounds (testing data).

fits the trend of kernel (Dirac) method better than C/d - the reason is explained in Section 3.2.

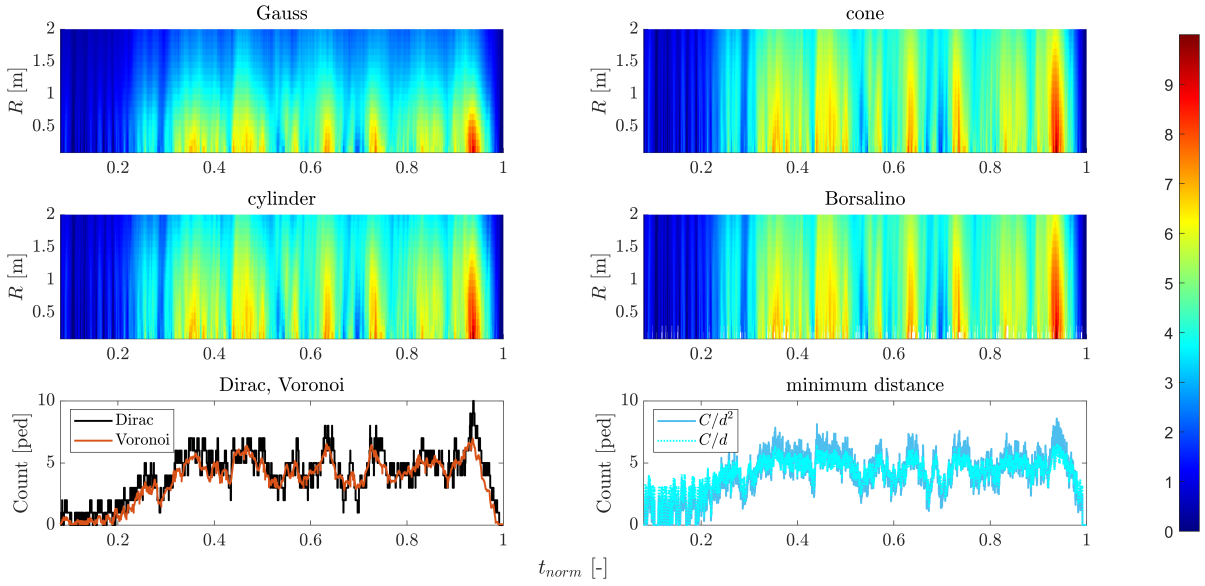


Figure 13. Pedestrian count with respect to time, kernel and its size (if it is possible).

4.7.2. Roughness and Featureless

Important density properties presented as roughness (2) and featureless (3) can be seen for round 6 of the experiment in Figure 14, or numerically in Table 2 and Table 3 in a detail for all methods for four different parametric sets (with rescaling Gaussian kernel) and different experimental rounds. The properties of minimum distance estimates are

depicted only in Figure 14 (right) – their roughness is denoted in Table 2 due to its high values outside of the scale of the figure.

The point approximation generates (as the most scattered curve with lots of jumps) an upper boundary for the other methods, except the roughness of the minimum distance estimates, see Figure 14 (left) and Table 2. It results from the fact that minimum distance distributions have very high peaks near real pedestrian locations. These peaks are similar to the peaks of density distribution of Dirac kernels, however the size of these peaks is variable in time because they are strongly affected by current pedestrian locations. Furthermore, Dirac kernel generates a constant section after every jump - the pedestrian count in the detector is not changing for several time steps, before another pedestrian leaves or comes to the detector. These deviations are cumulated in the roughness of the pedestrian count, thus the minimum distance estimate reaches much higher value than the point approximation.

Voronoi count can be interpreted as the median value for conic or cylindrical curves in the meaning of roughness, see Figure 14. Gaussian roughness confirms that Gaussian kernel is the most smoothed kernel shape (without any rescaling). Cylindrical kernel has very similar roughness as conic kernel, for low values of R is cylinder greater than cone - it is produced by the fact that cylinder is more similar to Dirac distribution than cone, especially for low values of R . Cylindrical kernel converges to the roughness of conic kernel for increasing R , if we exclude the trend from $R > 2.5$ m. This behaviour is caused by the size of the detector and a (very smoothed) pedestrian leaving this detector (and the rest of their kernel still being in the detector at the same time) - overall we may say that the larger the detector, the smaller the jump in the pedestrian count.

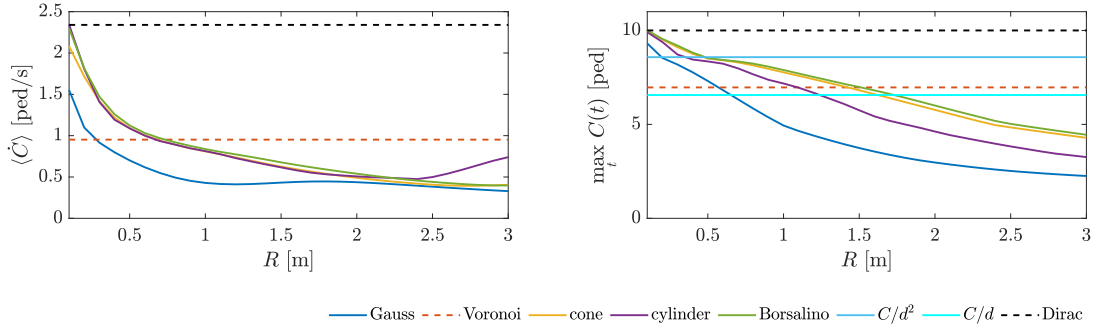


Figure 14. Left: roughness (the mean absolute derivative of the pedestrian count). Right: featureless (the maximum of the pedestrian count).

To discuss featureless, see Figure 14 (right) and Table 3. Gaussian kernel is the most smoothed kernel, thus its featureless has the lowest value from the all compared methods for every blur R . Due to the definition of the kernels, it is obvious that cone has greater featureless than cylinder for all values of R - the peak of conic pedestrian count is always higher than for cylindrical pedestrian count. Dirac has the greatest value of featureless and Voronoi represents the median featureless for conic, cylindrical and Borsalino kernel again. We can say for every kernel and every $t \in \mathbb{R}^+$ that

$$\max_t C_{\text{Dirac}}(t) \geq \max_t C_{\text{Borsalino}}(t) \geq \max_t C_{\text{Cone}}(t) \geq \max_t C_{\text{Cylinder}}(t) > \max_t C_{\text{Gauss}}(t).$$

The featureless of minimum distance estimates is similar as for Voronoi in the case of C/d and similar to kernel methods in the case of C/d^2 for $R < 1$ m.

We have examined roughness and featureless also for other experimental rounds and we have got very similar results and trends as for round 6. There is one fact to point out - although Dirac set the upper boundary for kernel methods for roughness and featureless in the round 6, it may not be fulfilled in general. It is possible under specific conditions to cross this boundary for other methods - for instance if there is $n \in \mathbb{N}$ pedestrians in the detector with the kernel size which enables them to be completely inside the detector, and (at least) one pedestrian outside the detector which is very close to the detector boundary with the kernel distribution which can enriched partially the count in the detector with $q \in \mathbb{Q}^+, q < 1$. Then the Dirac pedestrian count in the detector can be evaluated as n pedestrians, however the kernel pedestrian count in the detector is greater than n , specifically $n + q$ pedestrians. Nevertheless, this is a quite rare situation.

4.7.3. Mean Occupancy

The mean value of pedestrian count for all examined methods is found in Table 4. There is clearly seen that the conservation of the mean occupancy from Section 2.2 holds true through all examined methods for all examined parametric sets.

4.7.4. Example of Smoothing Techniques

As was mentioned in Section 2.3, there are two types of smoothing techniques which are depicted in Figure 15 for round 6. There is the curve of point approximation (Dirac kernel), conic kernel with $R = 0.9$ m and moving averages (averaging the values of point approximation belonging to one second). We can see the aforesaid equivalence of these smoothing techniques which is possible to calibrate to make the best correspondence.

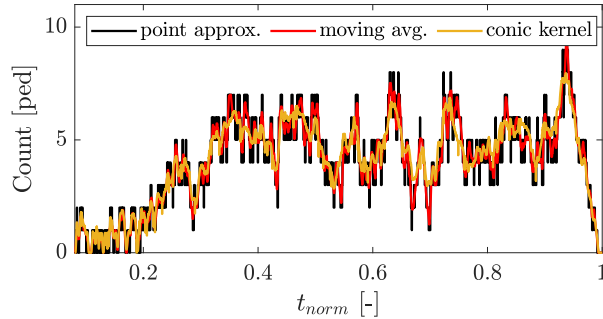


Figure 15. Example of different smoothing techniques: moving averages and kernel distribution.

Table 2. Summary of mean absolute derivative of pedestrian count for different method used for static detector.

$\langle \dot{C} \rangle$ [ped/s]		Training data for Min. distance				Testing data for Min. distance				
Method	R [m]	Rnd 5	Rnd 7	Rnd 4	Rnd 9	Rnd 2	Rnd 11	Rnd 6	Rnd 10	
NP	Voronoi	-	0.82	0.75	0.92	0.73	0.37	0.79	0.95	0.77
	Point approximation	-	2.25	2.46	2.36	2.35	1.87	2.53	2.34	2.62
	Minimum distance $1/d$	-	4.04	5.54	6.07	5.41	3.65	5.58	5.55	5.32
	Minimum distance $1/d^2$	-	8.54	12.78	12.35	12.17	5.80	12.80	12.41	12.24
P1	Conic kernel	0.3	1.60	1.27	1.49	1.26	1.42	1.28	1.42	1.28
	Cylindrical kernel	0.3	1.50	1.23	1.46	1.24	1.31	1.27	1.41	1.23
	Borsalino kernel	0.3	1.66	1.32	1.55	1.31	1.45	1.34	1.47	1.34
	Gaussian kernel	0.1	1.72	1.41	1.62	1.39	1.50	1.42	1.55	1.44
P2	Conic kernel	0.9	0.92	0.61	0.88	0.65	0.81	0.63	0.85	0.65
	Cylindrical kernel	0.9	0.88	0.56	0.88	0.61	0.72	0.59	0.85	0.62
	Borsalino kernel	0.9	0.96	0.65	0.91	0.68	0.85	0.66	0.88	0.67
	Gaussian kernel	0.3	1.02	0.70	0.95	0.73	0.92	0.72	0.92	0.72
P3	Conic kernel	1.5	0.66	0.38	0.64	0.43	0.50	0.41	0.63	0.43
	Cylindrical kernel	1.5	0.65	0.43	0.65	0.44	0.56	0.44	0.62	0.45
	Borsalino kernel	1.5	0.71	0.41	0.70	0.46	0.56	0.44	0.68	0.46
	Gaussian kernel	0.5	0.75	0.46	0.72	0.50	0.60	0.48	0.70	0.50

Table 3. Summary of maximum pedestrian count for different method used for static detector.

Max. ped. count [ped]		Training data for Min. distance				Testing data for Min. distance				
Method	R [m]	Rnd 5	Rnd 7	Rnd 4	Rnd 9	Rnd 2	Rnd 11	Rnd 6	Rnd 10	
NP	Voronoi	-	2.50	6.98	5.94	6.27	1.41	7.79	6.97	6.99
	Point approximation	-	5.00	9.00	8.00	9.00	4.00	9.00	10.00	9.00
	Minimum distance $1/d$	-	3.31	6.66	6.45	6.40	2.58	6.66	6.56	6.77
	Minimum distance $1/d^2$	-	4.65	8.52	8.33	8.38	3.41	8.53	8.58	8.67
P1	Conic kernel	0.3	4.76	7.98	7.52	8.10	3.28	8.41	9.11	8.40
	Cylindrical kernel	0.3	4.55	7.75	7.15	7.62	3.15	8.05	8.72	8.05
	Borsalino kernel	0.3	4.82	8.02	7.60	8.18	3.31	8.47	9.19	8.49
	Gaussian kernel	0.1	4.86	8.13	7.69	8.36	3.42	8.62	9.31	8.63
P2	Conic kernel	0.9	3.82	7.16	6.47	6.67	2.80	7.84	7.96	7.26
	Cylindrical kernel	0.9	3.54	6.90	6.22	6.26	2.59	7.51	7.37	7.00
	Borsalino kernel	0.9	3.89	7.25	6.52	6.76	2.85	7.92	8.08	7.30
	Gaussian kernel	0.3	4.02	7.37	6.56	6.88	2.89	7.92	8.18	7.46
P3	Conic kernel	1.5	3.17	6.48	5.74	5.89	2.34	7.03	6.82	6.50
	Cylindrical kernel	1.5	2.63	5.88	5.06	5.39	1.98	6.27	5.75	5.93
	Borsalino kernel	1.5	3.28	6.61	5.89	5.99	2.41	7.18	6.99	6.65
	Gaussian kernel	0.5	3.37	6.75	6.06	6.20	2.53	7.39	7.31	6.83

Table 4. Summary of mean pedestrian count for different methods used for static detector.

Mean ped. count [ped]		Training data for Min. distance				Testing data for Min. distance				
Method	R [m]	Rnd 5	Rnd 7	Rnd 4	Rnd 9	Rnd 2	Rnd 11	Rnd 6	Rnd 10	
NP	Voronoi	-	0.77	4.03	2.81	3.40	0.27	3.69	3.63	3.58
	Point approximation	-	1.51	4.29	3.34	3.80	0.68	4.18	4.05	4.01
	Minimum distance $1/d$	-	1.52	4.27	3.72	3.95	0.85	4.22	4.11	4.12
	Minimum distance $1/d^2$	-	1.46	4.21	3.49	3.82	0.73	4.12	4.04	4.00
P1	Conic kernel	0.3	1.59	4.49	3.48	3.99	0.73	4.35	4.26	4.21
	Cylindrical kernel	0.3	1.58	4.48	3.47	3.98	0.73	4.33	4.25	4.20
	Borsalino kernel	0.3	1.59	4.49	3.49	3.99	0.73	4.35	4.27	4.22
	Gaussian kernel	0.1	1.59	4.49	3.49	3.99	0.73	4.35	4.27	4.22
P2	Conic kernel	0.9	1.59	4.43	3.39	3.91	0.77	4.24	4.15	4.10
	Cylindrical kernel	0.9	1.60	4.37	3.33	3.84	0.81	4.15	4.07	4.00
	Borsalino kernel	0.9	1.59	4.44	3.40	3.93	0.76	4.26	4.16	4.12
	Gaussian kernel	0.3	1.58	4.44	3.41	3.93	0.75	4.27	4.18	4.13
P3	Conic kernel	1.5	1.52	4.19	3.17	3.65	0.78	3.94	3.89	3.81
	Cylindrical kernel	1.5	1.39	3.87	2.88	3.32	0.74	3.58	3.54	3.46
	Borsalino kernel	1.5	1.55	4.26	3.23	3.71	0.80	4.01	3.95	3.87
	Gaussian kernel	0.5	1.54	4.30	3.27	3.76	0.77	4.07	4.00	3.93

5. Conclusions

To conclude, the density (and pedestrian count) evaluated inside a detector significantly depends on the blur parameter R hidden inside an individual density distribution (kernel function). As shown in this study, desired behaviour of detector density from perspective of roughness (mean absolute derivative), featureless (pedestrian blending) and conservation of mean occupancy (stability in time) may be achieved by a specific setting of this parameter. Presented (symmetric) kernels may differ by scaling (e.g. conic kernel versus Gaussian kernel), however all of them converge (directly or after rescaling) to the similar value of density. The shape itself can be selected with respect to its essential qualities, implementation preferences or to fine-tune the density estimate.

Analysed non-parametric density evaluation methods (point approximation, Voronoi diagram, minimum distance estimate) bring similar values as the kernel methods with the appropriate value of blur parameter. To be more specific, the blur going to zero corresponds to the point approximation and the blur in interval $(1.5, 3)$ m fits the Voronoi method. In the range $(0.7, 1.2)$ m, the conic distribution corresponds to the density evaluated using the minimum distance to pedestrian. As theoretically derived and moreover illustrated on experimental data, it is more accurate to apply the minimum distance squared instead of the one-dimensional formula often used in vehicular traffic.

Research summarized in this article presents fundamental results for other work. Individual density distribution was used by author to quantify pedestrian *comfort* in civil engineering context in cooperation with Faculty of Civil Engineering, Brno University of Technology. The definition of comfort is based on density distributions in the way of median value over time. To find appropriate kernel size, proxemics zones were assumed (Hall (1959)) and 80 percent of the mass of the Gaussian kernel was chosen to fit into personal space (which was delimited by Hall). The rest of the kernel covers other proxemics zones. This definition gives reasonable findings according to preliminary results, the details of this project can be seen in Kratochvílová et al. (2022).

Finally, the further research would extend the presented work by the analysis of pedestrian surroundings, i.e. the study of the area affecting the pedestrian behaviour assuming the density distribution is already known. Besides, the set of methods estimating density analysed in this paper is not final – authors would seek for other techniques and extend the study both in width and depth.

Acknowledgement

This work was supported by the Ministry of Education, Youth, and Sports of the Czech Republic (MŠMT ČR) under Grant SGS21/165/OHK4/3T/14 and under project Center for Advanced Applied Science CZ.02.1.01/0.0/0.0/16-019/0000778.

Disclosure statement

The authors report there are no competing interests to declare.

References

- Baszczyńska, Aleksandra, et al. 2016. “Kernel Estimation of Cumulative Distribution Function of a Random Variable with Bounded Support.” *Statistics in Transition. New Series* 17 (3): 541–556.
- Bukáček, Marek, Pavel Hrabák, and Milan Krbálek. 2015. “Experimental analysis of two-dimensional pedestrian flow in front of the bottleneck.” In *Traffic and Granular Flow'13*, 93–101. Springer.
- Bukáček, Marek, Pavel Hrabák, and Milan Krbálek. 2016. “Individual microscopic results of bottleneck experiments.” In *Traffic and Granular Flow'15*, 105–112. Springer.
- Bukáček, Marek, Pavel Hrabák, and Milan Krbálek. 2018. “Microscopic travel-time analysis of bottleneck experiments.” *Transportmetrica A: transport science* 14 (5-6): 375–391.
- Bukáček, Marek, and Jana Vacková. 2019. “Evaluation of pedestrian density distribution with respect to the velocity response.” In *Traffic and Granular Flow'17*, Springer.
- Chacón, José E, and Tarn Duong. 2018. *Multivariate kernel smoothing and its applications*. Chapman and Hall/CRC.
- Daamen, Winnie, and Serge P Hoogendoorn. 2007. “Flow-density relations for pedestrian traffic.” In *Traffic and granular flow'05*, 315–322. Springer.
- Duives, Dorine C, Winnie Daamen, and Serge P Hoogendoorn. 2015. “Quantification of the level of crowdedness for pedestrian movements.” *Physica A: Statistical Mechanics and its Applications* 427: 162–180.
- Fan, Shimao. 2013. “Data-fitted generic second order macroscopic traffic flow models.” PhD diss., Temple University. Libraries.
- Fan, Shimao, Michael Herty, and Benjamin Seibold. 2013. “Comparative model accuracy of a data-fitted generalized Aw-Rascle-Zhang model.” *arXiv preprint arXiv:1310.8219* .
- Hall, E.T. 1959. “The Silent Language.” .
- Helbing, Dirk, Anders Johansson, and Habib Zein Al-Abideen. 2007. “Dynamics of crowd disasters: An empirical study.” *Physical review E* 75 (4): 046109.
- Helbing, Dirk, Anders Johansson, Joachim Mathiesen, Mogens H Jensen, and Alex Hansen. 2006. “Analytical approach to continuous and intermittent bottleneck flows.” *Physical review letters* 97 (16): 168001.
- Hillebrand, Arne, Han Hoogeveen, and Roland Geraerts. 2020. “Comparing different metrics quantifying pedestrian safety.” *Collective Dynamics* 5: 158–166.
- Johansson, Anders. 2009. “Data-driven modeling of pedestrian crowds.” .
- Johansson, Anders, Dirk Helbing, Habib Z Al-Abideen, and Salim Al-Bosta. 2008. “From crowd dynamics to crowd safety: a video-based analysis.” *Advances in Complex Systems* 11 (04): 497–527.
- Kerner, Boris S. 2004. “Three-phase traffic theory and highway capacity.” *Physica A: Statistical Mechanics and its Applications* 333: 379–440.
- Kratochvílová, Martina, Ondřej Uhlík, Jana Vacková, Jiří Apeltauer, Tomáš Apeltauer, and Jan Podroužek. 2022. “Efektivní časoprostorové predikce s využitím metod strojového učení.” *Průběžná zpráva za rok 2021 TAČR ZETA TJ04000232*.
- Krbálek, Milan, and Michaela Krbálková. 2018. “3s-Unification for Vehicular Headway Modeling.” *arXiv preprint arXiv:1811.05325* .
- Krisp, Jukka M, Stefan Peters, Christian E Murphy, and Hongchao Fan. 2009. “Visual bandwidth selection for kernel density maps.” *PGF-Photogrammetrie Fernerkundung Geoinformation* 5: 441–450.
- Liddle, Jack, Armin Seyfried, Bernhard Steffen, Wolfram Klingsch, Tobias Rupprecht, Andreas Winkens, and Maik Boltes. 2011. “Microscopic insights into pedestrian motion through a bottleneck, resolving spatial and temporal variations.” *arXiv preprint arXiv:1105.1532* .
- Mollier, Stéphane, Maria Laura Delle Monache, Carlos Canudas-de Wit, and Benjamin Seibold. 2019. “Two-dimensional macroscopic model for large scale traffic networks.” *Transportation Research Part B: Methodological* 122: 309–326.
- Plaue, Matthias, Günter Bärwolff, and Hartmut Schwandt. 2014. “On measuring pedestrian

- density and flow fields in dense as well as sparse crowds.” In *Pedestrian and Evacuation Dynamics 2012*, 411–424. Springer.
- Plaue, Matthias, Minjie Chen, Günter Bärwolff, and Hartmut Schwandt. 2012. “Multi-view extraction of dynamic pedestrian density fields.” *PGF Photogrammetrie, Fernerkundung, Geoinformation* 547–555.
- Predtetschenski, WM, and AI Milinski. 1971. “Personenströme in Gebäuden-Berechnungsmethoden für die Projektierung Rudolf Müller.” .
- Schadschneider, Andreas, Debashish Chowdhury, and Katsuhiro Nishinari. 2010. *Stochastic transport in complex systems: from molecules to vehicles*. Elsevier.
- Schadschneider, Andreas, Mohcine Chraïbi, Armin Seyfried, Antoine Tordeux, and Jun Zhang. 2018. “Pedestrian Dynamics: From Empirical Results to Modeling.” In *Crowd Dynamics, Volume 1*, 63–102. Springer.
- Schadschneider, Andreas, and Armin Seyfried. 2011. “Empirical results for pedestrian dynamics and their implications for modeling.” *Networks & heterogeneous media* 6 (3): 545.
- Silverman, BW. 1986. “Density Estimation for Statistics and Data Analysis, publisher Chapman and Hall.” *London, UK* .
- Steffen, Bernhard, and Armin Seyfried. 2010. “Methods for measuring pedestrian density, flow, speed and direction with minimal scatter.” *Physica A: Statistical mechanics and its applications* 389 (9): 1902–1910.
- Tordeux, Antoine, Jun Zhang, Bernhard Steffen, and Armin Seyfried. 2015. “Quantitative comparison of estimations for the density within pedestrian streams.” *Journal of statistical mechanics: theory and experiment* 2015 (6): P06030.
- Treiber, Martin, and Arne Kesting. 2013. “Traffic flow dynamics.” *Traffic Flow Dynamics: Data, Models and Simulation, Springer-Verlag Berlin Heidelberg* .
- Underwood, Robin T. 1960. “Speed, volume, and density relationships.” .
- Vacková, Jana, and Marek Bukáček. 2019. “The Microscopic Analysis of Velocity-Density Paradigm.” In *International Conference on Applied Mathematics 2019, APLIMAT*.
- Wand, Matt P, and M Chris Jones. 1994. *Kernel smoothing*. Chapman and Hall/CRC.